High-Resolution Tunnel Junction Extreme Ultraviolet Detectors Limited by Quasiparticle Counting Statistics

Stephan Friedrich, Johan B. le Grand, Lawrence J. Hiller, John Kipp, Matthias Frank, Simon E. Labov
Lawrence Livermore National Laboratory, P.O. Box 808, L-418, Livermore CA 94550, USA

Stephen P. Cramer
Lawrence Berkeley National Laboratory, 1 Cyclotron Road, MS 6-2100, Berkeley CA 94720, USA

Andrew T. Barfknecht
Conductus Inc., 969 W. Maude Avenue, Sunnyvale CA 94086, USA

Abstract — **Superconducting tunnel junctions (STJs) can be used as high-resolution high-count rate photon detectors. They are based on the measurement of the excess quasiparticle tunneling current caused by the absorption of a photon in one of the junction electrodes. We have fabricated Nb-Al-AlOx-Al-Nb tunnel junction detectors with different sizes and characterized them in sychrotron experiments. We present a study of the detector performance in the energy band between 50 and 1000 eV. For photon energies below 70 eV, the intrinsic device resolution of the best STJ devices agrees with the theoretical limit set by the statistics of the charge generation and tunneling processes.**

I. Introduction

High-resolution cryogenic x-ray detectors [1], [2] are being developed for a wide range of applications from material science [3] and microanalysis [4] to particle [5] and astrophysics [6] - [8]. Superconducting tunnel junctions (STJs) are one class of cryogenic x-ray detectors. They offer very high energy resolution (≈ few eV below 1 keV) at maximum count rates well above those of other cryogenic detectors (≈10,000 counts/s) [9]. STJs consist of two superconducting electrodes separated by a thin insulator. They utilize the small energy gap Δ by which excited single particle states (called quasiparticles) are separated from the Cooper pairs that constitute the superconducting electronic ground state. A photon with energy E is absorbed in one of the electrodes, breaks Cooper pairs and thereby generates a certain number of excess quasiparticles in proportion to its energy. These quasiparticles can tunnel through the insulating barrier, thus producing an excess current proportional to the energy of the incoming photon. The integrated excess charge Q provides a measure of the number of initially generated quasiparticles and thus of the incident photon energy according to [10], [11]

$$\frac{Q}{e} = \langle n \rangle \frac{E}{\varepsilon} \pm \langle n \rangle \sqrt{\frac{E}{\varepsilon}\left(F + 1 + 1/\langle n \rangle\right)}. \quad (1)$$

Here e is the electronic charge, $\varepsilon \approx 1.7\ \Delta$ [12] is the average energy required to generate a single excess quasiparticle, <n> is the average number of tunneling events each quasiparticle undergoes, and $F \approx 0.2$ [12] is the Fano factor that describes the statistical fluctuations in the initial charge generation process.

STJ detectors are different from conventional semiconductor Si(Li) or Ge detectors in that the energy gap Δ is of order 1 meV in superconductors, about a factor 1000 smaller compared to the gap in semiconductors. X-rays therefore generate roughly 1000 times more excess charge carriers in superconductors compared to semiconductors. Theoretically, this translates into an improved energy resolution by a factor $\sqrt{1000} \approx 30$, i.e. below 10 eV FWHM for photon energies up to 10 keV.

We are developing STJ detectors based on Nb-Al-AlOx-Al-Nb thin-film technology. We have tested their performance in the extreme ultraviolet (EUV) energy range between 50 and 70 eV. We find that the intrinsic device resolution agrees with the theoretical limit predicted by equation (1) within the error of the experiment. Previous experiments in the energy range between 0.2 and 1 keV have produced an intrinsic resolution exceeding the theoretical limit by 15%[13]. We speculate that the improved performance at low energy is due to complete photon energy relaxation in the Nb absorber, while higher-energy photons partially relax their energy in the Al film.

II. Operating Principle

The Nb-Al-AlOx-Al-Nb devices discussed here are fabricated at Conductus Inc. in Sunnyvale, CA, using a modified photolithographic trilayer process. They consist of a 265 nm bottom Nb film, an Al-AlOx-Al tunnel junction with 50 to

Manuscript received September 15, 1998

Funding for this research was provided by the DOE, Office of Biological and Environmental Research, by the NIH through grant No. GM 44380, and by NASA through SBIR Contract No. NAS5-32805 and through UV detector development grant No. NAG5-4137. This work was performed under the auspices of the U.S. Department of Energy by LLNL under contract No. W-7405-ENG-48 at the SSRL which is operated by the DOE, Office of Basic Energy Sciences.

Corresponding author: Friedrich1@llnl.gov

1051-8223/99$10.00

200 nm thick Al electrodes, and a 165 nm top Nb absorber. Device sizes vary between 35 μm × 35 μm and 100 μm × 100 μm. Details of this multilayer fabrication process have been published elsewhere [10], [14].

X-rays are captured in the top Nb electrode by photoelectric absorption. The resulting photoelectron relaxes its energy within 1 ns in a complicated cascade involving inelastic electron-electron and electron-phonon scattering and Cooper pair breaking by high-energy phonons [15]. At the end of the cascade about 60% of the x-ray energy has been converted into quasiparticles close to the Nb gap energy and about 40% has been converted into sub-gap phonons whose energy is no longer sufficient to break Cooper pairs.

When these quasiparticles diffuse from the Nb into the adjacent Al layer, where the superconducting gap is lower, they scatter inelastically to the Al gap energy [fig. 1]. This process is called trapping because it confines the charges to a region close to the tunnel barrier [16]. Trapping separates the absorber from the detector function of the device. The Nb absorber can be made thick for efficient absorption, subject to the constraint that the film stress due to lattice mismatch between Nb and Al does not reduce the quality of the AlOx tunneling barrier. The Al traps can be made thin for fast tunneling such that the excess charges can be detected before they again relax into their ground state. Trapping also increases the lifetime of the quasiparticles, as it keeps them away from the possibly degraded detector surface.

Trapped quasiparticles can undergo two types of tunneling processes [17]. They can tunnel directly from one electrode to the counterelectrode whenever they face empty available states on the opposite side of the tunnel barrier [figure 1, process 1]. Once they scatter down to the gap energy in the counterelectrode, this direct tunneling process is no longer possible, because these charges now face the energy gap in the opposing electrode. However, if a confining potential on either side of the barrier prevents the quasiparticles from diffusing out into the leads, they can still contribute to the tunneling current by breaking a Cooper pair in the opposing electrode and forming a new pair with one of the now unpaired electrons in the counterelectrode [figure 1, process 2]. This process (called backtunneling) moves a charge in the *same* direction across the tunneling barrier as the direct tunneling process, while returning an unpaired particle *back* to the other electrode. Both processes occur at the same tunneling rate $1/\tau_{tunn}$. Quasiparticles can engage in both tunneling processes until they ultimately recombine and form Cooper pairs again after the characteristic recombination time τ_{rec}. Backtunneling thus provides an intrinsic charge amplification by a factor given by the average number of tunneling events $\langle n \rangle = \tau_{rec}/\tau_{tunn}$ each quasiparticle undergoes. Since the number of tunneling events is subject to statistical fluctuations, this charge amplification process also adds statistical noise to the tunneling current (cf. equation 1) [10], [11]. Since backtunneling increases both the signal and the noise, it is desirable in STJ detectors only as long as the electronic noise contributes an appreciable fraction

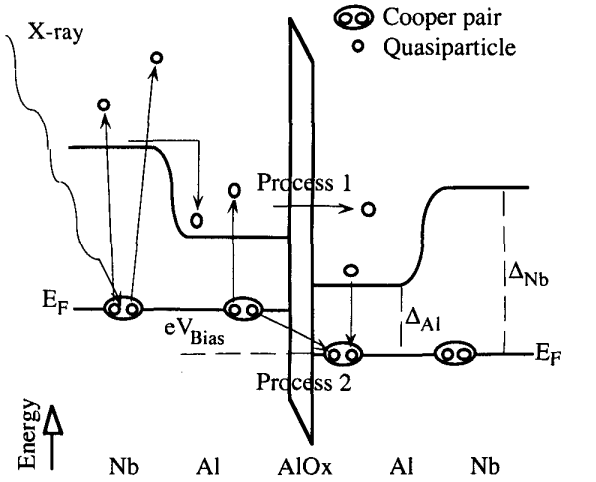

Fig. 1. Energy gap profile Δ(x) inside a tunnel junction detector. An x ray breaks Cooper pairs in the Nb absorber thereby generating free quasiparticles, which scatter into the Al trap and produce a current pulse by direct tunneling (process 1) and backtunneling (process 2).

to the resolution. Once the electronic noise is negligible, backtunneling reduces the ultimate detector resolution and should be suppressed. The devices discussed in this paper amplify the signal by a factor 3.1 through backtunneling. This limits the ultimately attainable linewidth to 1.0 - 4.6 eV FWHM for x-ray energies between 0.05 and 1 keV.

The tunneling rate $1/\tau_{tunn}$ for both direct and backtunneling depends on the density of available states to tunnel into. Since the density of states in a superconductor is strongly energy dependent (it diverges at the gap and decreases to the normal state value over an energy range of a few Δ), the tunneling rate depends on the charge distribution in the junction electrodes and on the bias voltage [18]. This gives rise to a voltage-dependent charge amplification factor $\langle n \rangle = \tau_{rec}/\tau_{tunn}$ and thus a voltage-dependent signal-to-noise ratio. The optimum bias voltage for each STJ detector is determined by maximizing the signal height in a bias region of low electronic noise. In the devices discussed here, the optimum bias voltage ranges from 260 to 380 μV.

III. Experimental Results

The STJ detectors are operated in a liquid helium cryostat with an adiabatic demagnetization refrigerator (ADR) stage. The ADR attains a base temperature of 60 mK, has a hold time of 8 hours below 0.4 K and requires about 30 minutes to cycle. A magnetic field of order 100 Gauss is applied parallel to the wafer in direction of the junction diagonal to suppress the dc Josephson current. We attach the ADR to the low-flux synchrotron beam line 1-1 at the Stanford Synchrotron Radiation Laboratory (SSRL) and illuminate the STJ detector directly with the monochromatic synchrotron beam. To prevent infrared (IR) radiation from heating the ADR stage, we use 1000 Å Al IR blocking windows. Photon absorption at the Al L edge limits the EUV measurements to energies below

72 eV, while the output of the monochromator at beam line 1-1 restricts the measurements to energies above 40 eV. We have verified that the monochromator is calibrated to ± 1 eV by scanning the incident beam through the Al L edge at 72 eV and observing a sharp drop in the count rate. All devices discussed here were made in the same fabrication run on the same wafer. For details of the experimental setup, see [9].

A. Energy Dependence

Figure 2 shows the spectral response of a 50 × 50 μm^2 STJ detector to monochromatic photons with an energy of 70 eV. A Gaussian fit matches the central peak well and yields an energy resolution ΔE = 1.90 ± 0.08 eV FWHM. The noise contribution from the readout electronics is ΔE = 1.39 ± 0.01 eV. The main uncertainty in determining the energy resolution arises from the ambiguity how to subtract the background from the peak.

This background is due to a residual SiO_2 surface layer on top of the Nb absorber that has not been completely removed in the fabrication process. Recent devices, in which this SiO_2 surface layer has been removed completely, no longer show this low energy artifact [19]. For the EUV data we still chose to examine devices from the same wafer we had used for the 0.2 to 1 keV data to make a more conclusive comparison with the higher energy data.

The detector resolution as a function of energy is shown in figure 3. It varies between 1.7 and 8.9 eV between 0.05 and 1 keV. The intrinsic device resolution (circles) is calculated by subtracting the electronic noise (dotted lines) and the monochromator line width (dashed line) in quadrature from the measured device resolution (squares). The electronic noise in the EUV measurements is less because of recent improvements in the readout electronics, which now employ a dc voltage biasing scheme [7].

We find that the intrinsic resolution of the STJ detector between 50 and 70 eV agrees with the theoretical limit as given by (1) to within the accuracy of the measurement. For

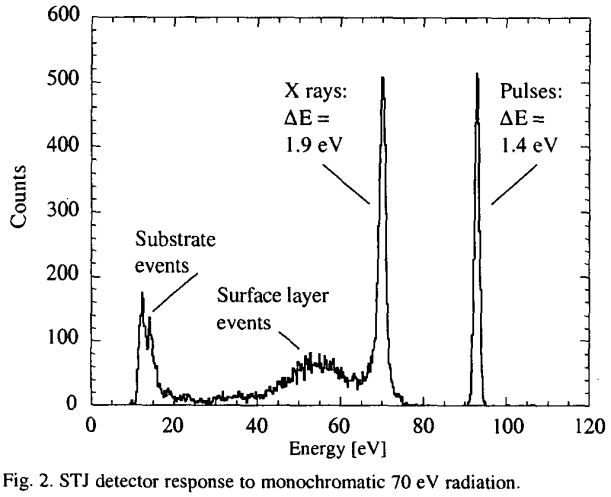

Fig. 2. STJ detector response to monochromatic 70 eV radiation.

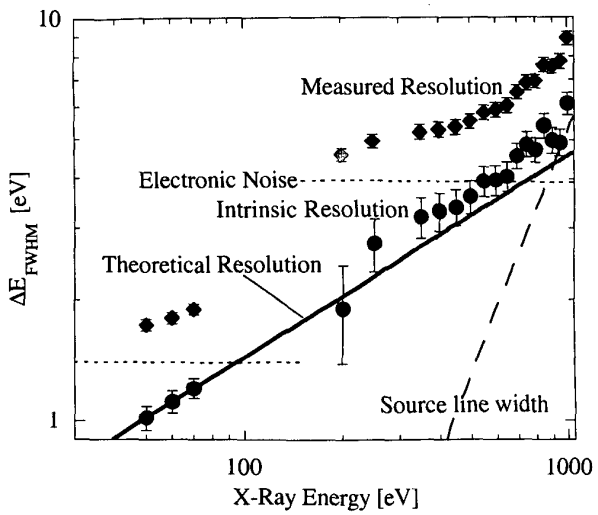

Fig. 3. STJ detector resolution as a function of energy. The intrinsic device resolution(circles) is calculated by subtracting electronic noise (dotted lines) and monochromator line width (dashed line) in quadrature from the measured resolution (squares). The solid line is the theoretical resolution limit $\Delta E_{FWHM} = 2.355\sqrt{\varepsilon E(F+1+1/\langle n\rangle}$ acc.to eqn. (1) for <n> = 3.1.

comparison, older measurements in the energy range between 200 and 1000 eV are included in figure 3 [13]. A fit to the intrinsic device resolution in that energy range shows a discrepancy of 15% between the experimental and the theoretical value. We speculate that this discrepancy is due to partial photon energy relaxation in the Al film. So far, all simulations of the initial energy relaxation process have assumed a homogeneous superconductor and have predicted a Fano factor F ≈ 0.2. This assumption may be justified even for an Nb/Al bilayer, provided that the energy of the incident photon is sufficiently low such that photon absorption and subsequent quasiparticle generation occur far from the Nb/Al interface. For photons above 100 eV this assumption starts to break down. Models of the initial charge generation process for different photon energies and different Nb/Al film thicknesses are currently being developed in order to better understand the effective Fano factor in bilayers [19].

B. Size Dependence

Spectroscopists often face a trade-off between optimum detector resolution and maximum device area. There are several size-dependent effects which influence the STJ detector resolution. Increased device capacitance increases the electronic noise and thus the practically attainable resolution. Spatial variations of the detector response may contribute more significantly to the line broadening in large devices. Furthermore, the perimeter-area-ratio affects the quasiparticle lifetime and thus the charge amplification factor $\langle n\rangle = \tau_{rec}/\tau_{tunn}$. This is because in STJs the lifetime is reduced from its thermal equilibrium value by regions of reduced gap, which serve as local trapping sites that remove

quasiparticles from the detection process. Depending on the fabrication process, the dominant trapping sites are located either along the perimeter of the STJ or spread out uniformly throughout the junction area. Finally, the device area affects the location of Fiske mode resonances. Fiske modes occur whenever the ac Josephson effect can excite a cavity resonance in the barrier region between the two electrodes. Fiske modes therefore depend on the bias voltage, the applied magnetic field and the junction area [21]. Biasing an STJ detector in the vicinity of a Fiske mode resonance increases the noise. Since the presence of a Fiske mode can affect the electronic noise more significantly than the device impedance and the shot noise, different size detectors show optimum performance at different bias voltages and thus for different charge amplification factors and different levels of electronic noise. This effect explains the non-monotonic dependence of electronic noise on device area at the bias point of optimum detector performance.

Figure 4 shows a data set examining the detector resolution as a function of device area for 60 eV photons. All four devices were made on the same wafer in the same fabrication run and are located within 2 mm of each other. The device resolution degrades faster with increasing device area than can be explained by the electronic noise contribution alone. This indicates that some additional broadening mechanism, most likely a spatially varying detector response, affects the detector resolution. Increased device homogeneity may still improve the detector response for large area devices.

IV. Discussion

STJ detector technology is now sufficiently mature to be used in novel scientific experiments. Initial applications are being pursued in astronomy [8], particles physics [5] and microanalysis [3]. As cryodetectors gain acceptance in the wider science community, additional applications in biophysics [19] and material science will also become important.

At present, there are two main limitations to our STJ detector system. The first is due to the finite absorption efficiency of the top 165 nm Nb film. Above ≈600 eV, this layer is no longer completely opaque and a certain fraction of the x rays is absorbed in the bottom Nb film. Since the response of the two layers can be slightly different, monochromatic lines can appear broadened or even split above ≈600 eV. Simply increasing the Nb absorber thickness is not possible, because the lattice mismatch between Nb and Al would increase the stress on the AlOx tunnel barrier and compromise its integrity. Our future devices will employ Ta rather than Nb absorbers for higher efficiencies at higher energies.

The second limitation is due to the small detector size. For fluorescence experiments, the sample must be placed within less than 1 cm of the detector in order to cover an appreciable solid angle. We are currently developing 3 by 3 arrays of 200 μm × 200 μm STJs to increase the solid angle by an order of magnitude. Future experiments will also use x-ray focusing optics to further increase the detector efficiency [4].

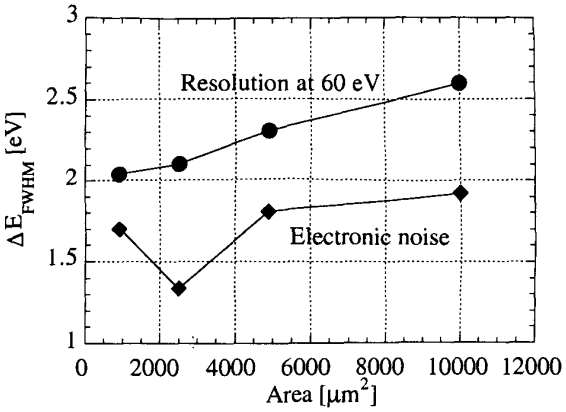

Figure 4: STJ detector resolution as a function of device area.

V. Summary

We have developed Nb-based superconducting tunnel junction (STJ) EUV and soft x-ray spectrometers. They have an energy resolution between 1.7 and 8.9 eV FWHM for photon energies between 0.05 and 1 keV at count rates up to ≈10,000 counts/s. When corrected for electronic noise and photon source line width, the resolution approaches the theoretical limit set by quasiparticle counting statistics. STJ spectrometers will significantly improve detection limits for the analysis of dilute samples and for L- and M-edge spectroscopy where line overlap can be a limiting problem.

References

[1] N.E. Booth, D.J. Goldie, *Supercond. Sci. Technol.*, vol. 9, pp. 493-516, 1996
[2] D. Twerenbold, *Rep. Prog. Phys.*, vol. 59, pp. 349-426, 1996
[3] M. Frank et al., *J. Synchrotron Rad.*, vol. 5, pp. 515-517, 1998
[4] D.A. Wollman, K.D. Irwin, G.C. Hilton, L.L. Dulcie, D.E. Newbury, J.M. Martinis, *J. Microscopy*, vol. 188, pp. 196-223, 1997
[5] S.W. Nam et al., *Nucl. Inst. Meth.* A, vol. 370, pp. 187-189, 1996
[6] D. McCammon et al., *Nucl. Inst. Meth.* A, vol. 370, pp. 266-268, 1996
[7] S. Friedrich et al., *IEEE Trans. Appl. Supercon.*, vol. 7, pp. 3383-3386 1997
[8] A. Peacock et al., *Nature*, vol. 381, pp. 135137, 1996
[9] M. Frank et al., *Rev. Sci. Inst.*, vol. 69, pp. 25-31, 1998
[10] C.A. Mears, S.E. Labov, A.T. Barfknecht, *Appl. Phys. Lett.*, vol. 63, pp. 2961-2963, 1993
[11] D.J. Goldie et al., *Appl. Phys. Lett.*, vol. 64, pp. 3169-3171, 1994
[12] N. Rando et al., *Nucl. Inst. Meth.*, vol. 313, 173-176, 1992
[13] J.B. le Grand et al., *Appl. Phys. Lett.*, vol. 73, 1295-1297, 1998
[14] A.T. Barfknecht, R.C. Ruby, H. Ko, *IEEE Trans. Magn.*, vol. 27, pp. 3125-3128, 1991
[15] A. Zehnder, *Phys. Rev.* B, vol. 52, pp. 12858-12866, 1995
[16] N.E. Booth, *Appl. Phys. Lett.*, vol. 50, pp. 293-295, 1987
[17] K.E. Gray, *Appl. Phys. Lett.*, vol. 32, pp. 392-395, 1978
[18] S. Friedrich et al., *Appl. Phys. Lett.*, vol. 71, pp. 3901-3904, 1997
[19] S. Friedrich et al., *J. Electron Spectr. and Rel. Phenomena* (1999), in press
[20] L.J. Hiller, Lawrence Livermore National Lab, in preparation
[21] R.E. Eck, D.J Scalapino, B.N. Taylor, *Proc. 9th Conf. Low Temp. Phys.*, pp. 415-420, 1965; J.G. Daunt (ed.), Plenum Press (New York)